Full Hamiltonian modelling of the two qubit devices

Author	Affiliation	Email
Alfredo Levy Yeyati	UAM	a.l.yeyati@uam.es
Sunghun Park		Sunghun.park@uam.es
Project Number	**Project Start Date**	**Duration**
828948	01.04.2019	48 Months
Classification		
	PU	
File Name		
WP No	**Work Package Name**	
5	Supporting theory	
Deliverable No	**Deliverable Name**	
D5.4	Full Hamiltonian modelling of the two qubit devices	
	Approved by	
	Steering Committee of the action	

The opinions expressed in the document are of the authors only and no way reflect the European Commission's opinions. The European Union is not liable for any use that may be made of the information. This project has received funding from the European Union's Horizon 2020 research and innovation programme under grant agreement No 828948.

DOCUMENT REVISION HISTORY

Revision	Date	Description	Author
1.0			

Table of Contents

1. Introduction

Andreev qubits can be coupled using the coupling schemes already designed for conventional superconducting qubits [Rigetti,Bertet,Chen]. As in the case of flux qubits Andreev qubits can be coupled inductively. One of such schemes is illustrated in Fig. 1a, where the intermediate circuit corresponds to a tunable mutual inductance [Chen].

The hybrid nanowires allow, however, to explore novel schemes like the one In Fig 1b and 1c. In these schemes the junctions are defined along the same nanowire. Fluxes ϕ_1 and ϕ_2 control the phase difference on the junctions defining the qubits while the gate potentials V_{g1}, V_{g2} and V_{gc} would allow to control the electron density on each junction. Such scheme would allow for tunable coupling without introducing additional microwave transmission lines like in [chen] and thus reducing drastically the distance between qubits (from the 100 mu to 100 nm scale).

In the present deliverable we present results on the microscopic modelling of two Andreev qubits based on a design like the ones of Fig. 1b and 1c. To simplify we focus on the short junction limit where each qubit is characterized by a single pair of Andreev levels and the spin-splitting is negligible.

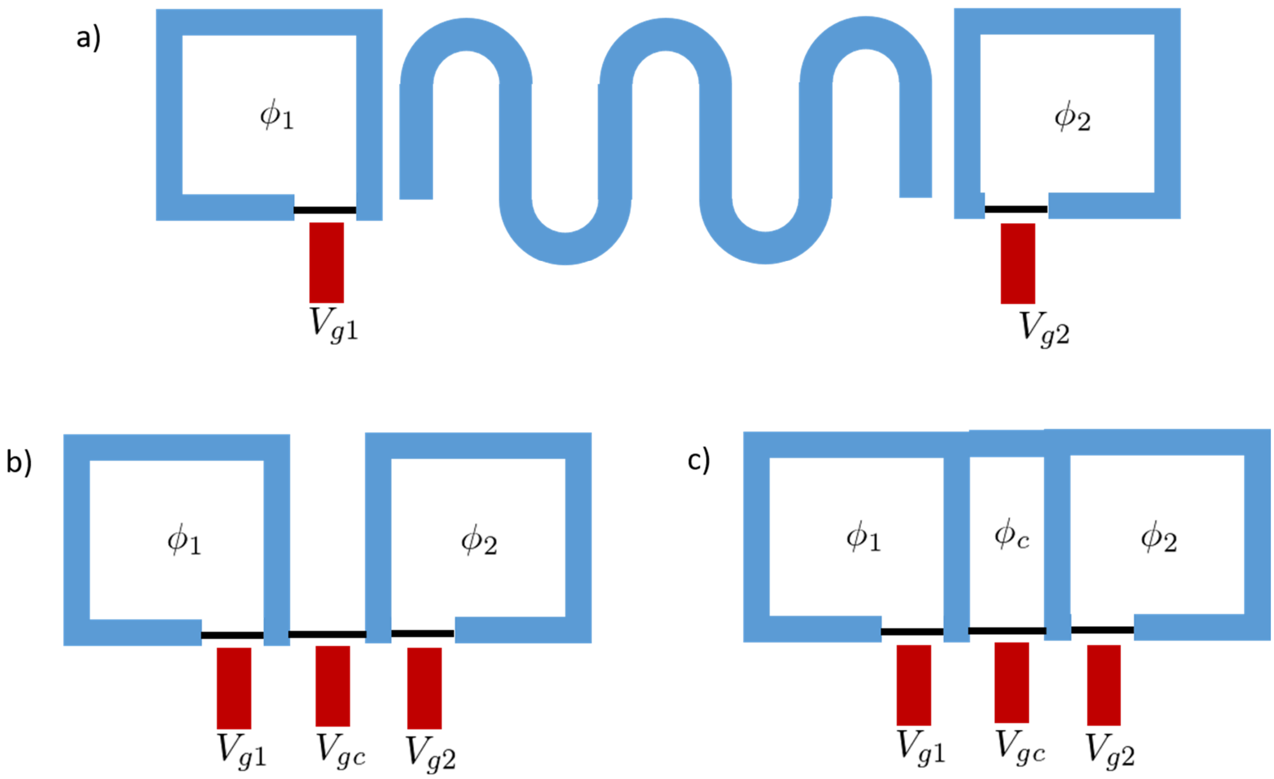

Fig. 1: *Different two-qubit coupling schemes. a) The qubits defined on two distant superconducting loops are coupled by a central transmission lines which behaves as a tunable inductance as in Ref. [Chen]. b)The two qubits are defined on the same nanowire. The charge densities on the three junctions are tunable by means of the gate electrodes 1, 2 and c. c) Same as b) but with an additional flux to control the phase difference on the central junction.*

2. Minimal model

We first analyze a minimal model for this type of design. Assuming for simplicity that the junctions are in the short limit (L <<ξ, where ξ is the superconducting coherence length) we model the qubits as spin-degenerate single levels coupled to superconducting leads, described by the following Hamiltonian,

$$H_0 = \sum_{i=1,2;\sigma} \varepsilon_i n_{i_\sigma} + 2\sum_{i=1,2} \Gamma_i \cos\frac{\phi_i}{2} d_{i\uparrow} d_{i\downarrow} \; + h.c.,$$

where d_{i_σ} are annihilation operators for fermions in qubit $i = 1{,}2$ and spin σ; and $n_{i_\sigma} = d^+_{i\ \sigma} d_{i_\sigma}$. The parameters Γ_i describe the coupling to the superconducting leads, which controls the induced pairing in the normal regions. Within this model each qubit is characterized by a pair of Andreev states $\pm E_{A_i}(\phi_i)$,with $E_{A_i} = \sqrt{\varepsilon_i^2 + 4\Gamma_i^2 \cos^2\frac{\phi_i}{2}}$.

The qubit-qubit coupling through the central region is due to a weak overlap of the Andreev states wave-functions that allows for quasiparticle tunneling, which is described by

$$V = \sum_\sigma t_{ec} d^+_{1,\sigma} \; d_{2,\sigma} + \sigma t_{car} d_{1,\sigma} \; d_{2.-\sigma} + h.c. \; ,$$

where t_{ec} and t_{car} denote the elastic cotunneling and the crossed Andreev amplitudes, which are such $t_{ec}, t_{car} \ll \Gamma_i$. These processes lead to an effective coupling between the qubits Andreev states. We now evaluate this coupling at the crossing where the two qubits states are degenerate. To simplify we consider a symmetric situation $\varepsilon_{1,2} = \varepsilon$ and $\Gamma_{1,2} = \Gamma$. In a Nambu basis $(d_{1\uparrow} d^+_{1\downarrow} d_{2\uparrow} d^+_{2\downarrow})$ the decoupled Andreev states wave-functions are given by $\Psi_1^+ = (\cos\theta_1 \sin\theta_1 \; 0 \; 0)$and $\Psi_2^+ = (0 \;\; 0 \;\; \cos\theta_2 \sin\theta_2)$ where

$$\tan\theta_i = \frac{E_A(\phi_i) - \varepsilon}{2\Gamma \cos\frac{\phi_i}{2}}$$

Then, at the degeneracy point $\phi_{1,2} = \phi$ and for real t_{ec}

$$< \Psi_1^+ |V| \Psi_2^+ > = \; t_{ec} \cos 2\theta + Re(t_{car}) \sin 2\theta \; .$$

This simple model suggests that the coupling can be tunable in several different ways. On the one hand, by depleting the central region by means of the central gate potential both t_{ec} and t_{car} could be reduced to zero. Another interesting possibility would be to use the fluxes as tuning parameters to reach the condition where $< \Psi_1^+ |V| \Psi_2^+ > = 0$ as a consequence of the interference between the cotunneling and crossed Andreev processes. Notice that this condition does not imply complete isolation of the two qubits but rather decoupling between the excited states $\Psi_{1,2}^+$. The ground states are given by $\Psi_1^- = (-\sin\theta_1 \; \cos\theta_1 \quad 0 \; 0)$ and $\Psi_2^- = (0 \;\; 0 \;\; -\sin\theta_2 \cos\theta_2)$, so that the coupling between the excited and the ground states at the degeneracy point is given by

$$< \Psi_1^- |V| \Psi_2^+ > = \; -t_{ec} \sin 2\theta + Re(t_{car}) \cos 2\theta + iIm(t_{car}).$$

By tuning the matrix elements$< \Psi_1^{+,-} |V| \Psi_2^{+,-} >$one could thus perform different two-qubit operations.As in the present minimal model t_{ec} and t_{car} are just phenomenological parameters, in the following we will explore these possibilities using a more microscopic description of the nanowire junctions.

3. Microscopic tight-binding model

We now model the designs of Fig. 1b and 1c using a single chain tight-binding model with position dependent on-site and superconducting pairing parameters, i.e.

$$H = \sum_{i,\sigma} \varepsilon_i c^+_{i,\sigma} c_{i,\sigma} + \sum_{i,\sigma} t_i c^+_{i,\sigma} c_{i+1,\sigma} \; + h.c. + \sum_i \Delta_i e^{-i\phi_i} c^+_{i,\uparrow} c^+_{i,\downarrow} \; + h.c.$$

in order to describe, the effect of the gates V_{g1}, V_{gc}, V_{g2} and the normal ($\Delta_i = 0$) and superconducting regions ($\Delta_i = 0.185 meV$) respectively. The phase difference between superconducting regions is controlled with $\phi_i(\phi_{i\epsilon S1} = 0, \phi_{i\epsilon Sc1} = \phi_1, \; \phi_{i\epsilon Sc2} = \phi_1 + \phi_c, \; \phi_{i\epsilon S2} = \; \phi_1 + \phi_c + \phi_2)$. The lattice parameter is$a = 10nm$, and on-site ($\varepsilon_i \lesssim 2t_0/a^2$) and hopping ($t_i = t_0/a^2 \; = \hbar^2/(2m^* a^2)$) parameters correspond to a discretization of a slightly populated typical semiconductor nanowire with $m^* \sim 0.02 m_e$.

For a concrete realization we take the lengths of the normal regions from left to right to be $90, 100$, and $120\,nm$ in order to account for possible experimental imperfections; similarly for the superconducting ones, with $600, 250, 350$, and $600\,nm$. Figure 2 (left) shows the resulting spectrum of Andreev states varying ϕ_1 with fixed ϕ_c and ϕ_2, and compares it with results from the minimal model fitted near the avoided level crossing (dashed lines). The remaining subfigures depict the evolution of the wave-function for the lowest Andreev state as ϕ_1 moves along the level crossing, displaying the switching of its localization from the right to the left qubit.

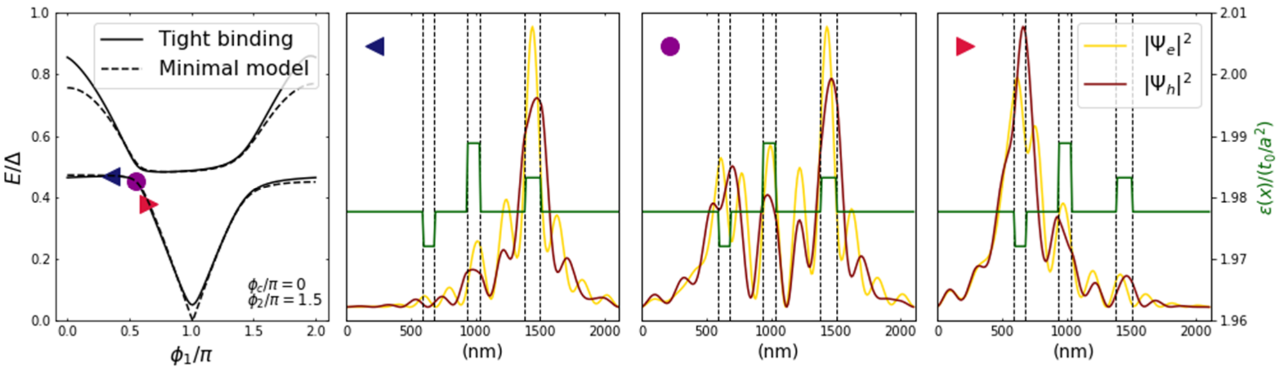

Fig. 2. *Tight-binding wave-function switch from right to left qubit as ϕ_1 moves across the level crossing for the setup of Fig. 1b. Dashed lines in left panel correspond to the minimal model fitted near the crossing. Green lines in the wave-functions plots represent the on-site energies, modulated with the gates. Vertical dashed lines separate normal and superconducting regions. The central phase difference ϕ_c is set to zero.*

4. Low energy model with scattering matrix approach

Here we present a low energy Hamiltonian for the design of Fig. 1c and Fig. 3a by using scattering matrix method. We consider a setup shown in Fig. 3b where the two qubits 1 and 2 have low Andreev energy states with high transmission probabilities T_i around the phase difference $\phi_i = \pi$ such that they are coupled via a qubit in the middle with high Andreev energy resulting in an effective coupling between the two qubits. The Hamiltonian given by

$$H_{eff} = \begin{pmatrix} H_1 & 0 \\ 0 & H_2 \end{pmatrix} + \begin{pmatrix} V_{1c} G_c^0 V_{1c}^+ & V_{1c} G_c^0 V_{2c}^+ \\ V_{2c} G_c^0 V_{1c}^+ & V_{2c} G_c^0 V_{2c}^+ \end{pmatrix},$$

where the qubit Hamiltonian H_i and the Green's function for the middle junction G_c^0 are

$$H_i = \begin{pmatrix} E_{Ai} & 0 \\ 0 & -E_{Ai} \end{pmatrix}, \qquad G_c^0 = (E - H_c)^{-1} \approx \begin{pmatrix} -E_c^{-1} & 0 \\ 0 & E_c^{-1} \end{pmatrix},$$

where we assumed that the energy regime we are interested in is much smaller than the Andreev energy of the middle qubit, $|E| \ll E_c$. V_{ic} and V_{ic}^+ are two by two matrices describing the overlaps of wave functions between i-junction and the middle junction,

$$V_{ic} = \begin{pmatrix} t_{++}^{ic} & t_{+-}^{ic} \\ t_{-+}^{ic} & t_{--}^{ic} \end{pmatrix}, \; t_{ss'}^{ic} = \langle \Psi_i^s | H_\Delta | \Psi_c^{s'} \rangle.$$

where $|\Psi_i^s\rangle$ with $s = \pm$ is the decoupled Andreev state of energy $E = s\, E_{Ai}$ and H_Δ is the Hamiltonian for the superconducting gap in the region where the overlap occurs. The modification due to the presence of the middle junction consists of two parts: (1) the Andreev energy of each qubit is modified as follows,

$$\widetilde{H}_i = H_i + V_{ic} G_c^0 V_{ic}^+.$$

Fig. 3c shows the Andreev energies E_1 of $\widetilde{H}_1$ for different values of the phase difference ϕ_c. For clarity, the energy for the unperturbed qubit 1 is illustrated by dashed lines. The dependence on ϕ_c is the same for $\widetilde{H}_2$.
(2) The coupling between qubits 1 and 2 is described by the term

$$V = V_{1c} G_c^0 V_{2c}^+,$$

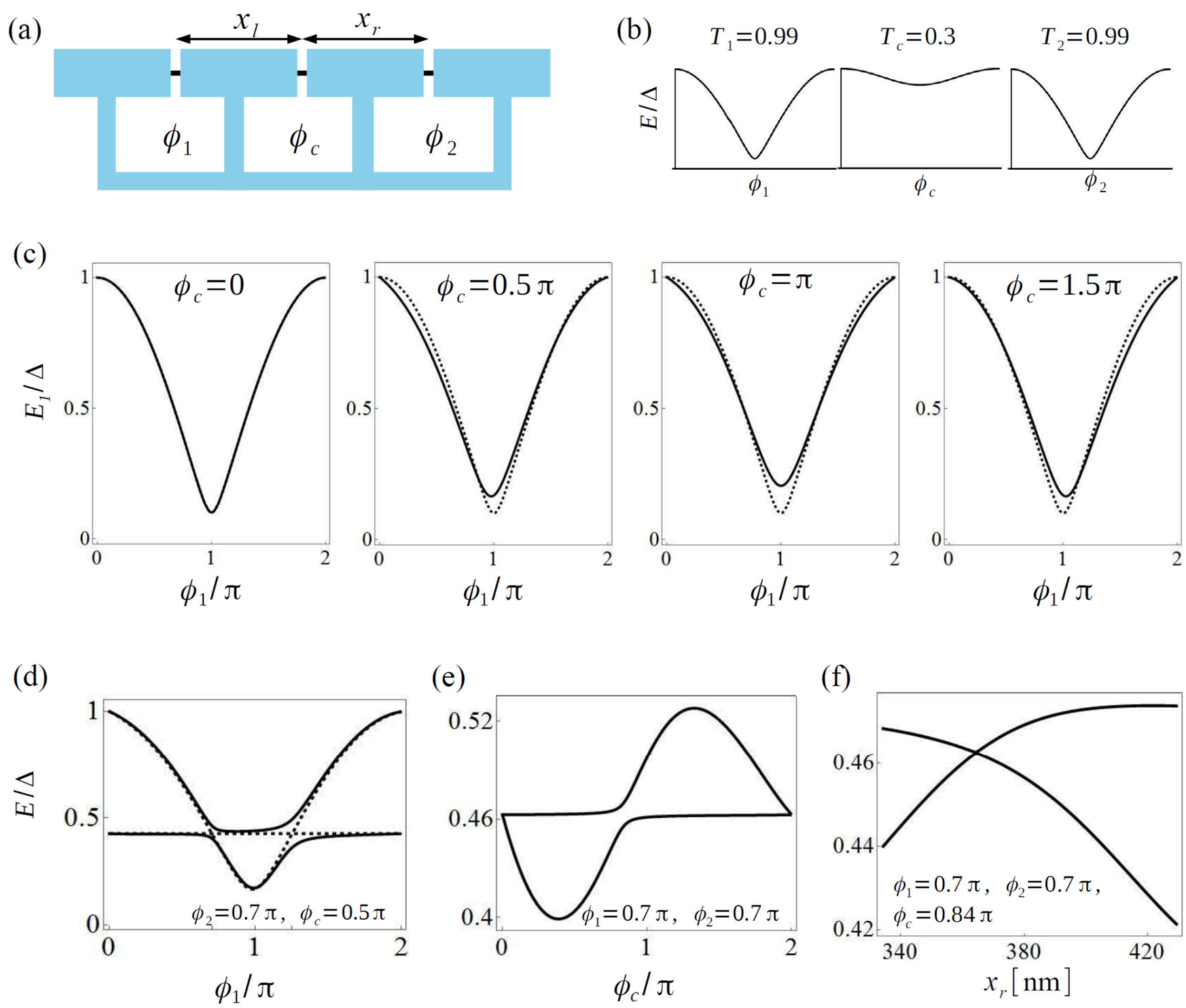

Fig. 3. *Low energy model for the coupled two qubits. (a) Schematic of the experimental setup which is the same as in Fig. 1(c). x_l and x_r are the distances of the qubits 1 and 2 from the middle junction. (b) Andreev energies of the junctions in the absence of coupling between them. Qubits 1 and 2 with high transmission probabilities T_1 and T_2 are coupled via the middle qubit with low transmission T_c. (c) Andreev energy of qubit 1 for different values of ϕ_c by solving the perturbed Hamiltonian $\widetilde{H}_1$ due to the presence of the junction in the middle. Dashed curves indicate the unperturbed Andreev energy E_{A1}. (d), (e) and (f) are results obtained by solving the low energy Hamiltonian. Dashed curves in (d) correspond to the energy eigenvalues of $\widetilde{H}_i$ without the coupling V. Here $x_l = x_r = 380$nm are used in (c) and (d) and $x_l = 380$nm in (e).*

which induces the energy splitting. Note that the direct coupling between the qubits 1 and 2, which becomes important at $\phi_c = 0$ and 2π, is neglected in our effective model, and thus, the coupling term V is valid away from the values of ϕ_c. Fig. 3d shows the anti-crossings between the energy levels of qubits 1 and 2 around at $\phi_1 = 0.7\,\pi$ and $1.3\,\pi$. Their magnitudes of the anti-crossing gaps are asymmetric.

To understand the asymmetry of the anti-crossing gaps in Fig. 3d, which we refer to as the left gap δE_L and right gap δE_R with respect to $\phi_1 = \pi$, we analyze the matrix element of the coupling,

$$|\langle \Psi_1^+ | V | \Psi_2^+ \rangle| = \frac{1}{E_c} \left| t_{++}^{1c}\, t_{++}^{2c\,*} - t_{+-}^{1c}\, t_{+-}^{2c\,*} \right|.$$

In the ballistic limit $T_{1,2} = 1$, the matrix element at the crossing point $\phi_1 = \phi_2$ and $\phi_1 = 2\pi - \phi_2$ can be expressed as

$$|\langle \Psi_1^+ | V | \Psi_2^+ \rangle|(\phi_1 \sim 0.7\,\pi) = \frac{\sqrt{\Delta^2 - E_c^2}}{2\,\xi^2} F(x_l, x_r) \sin\frac{\phi_2}{2} \cos\frac{\phi_2}{2},$$
$$|\langle \Psi_1^+ | V | \Psi_2^+ \rangle|(\phi_1 \sim 1.3\,\pi) = \frac{\sqrt{\Delta^2 - E_c^2}}{2\,\xi^2} F(x_l, x_r) \sin\frac{\phi_2}{2},$$

where ξ is the superconducting coherence length and $F(x_l,\ x_r)$ is given by

$$F(x_l, x_r) = \left[\frac{\exp(-q_1 x_l) - \exp(-q_c x_l)}{q_c - q_1}\right]\left[\frac{\exp(-q_2 x_r) - \exp(-q_c x_r)}{q_c - q_2}\right].$$

Here, $q_i = (1/\xi)\sqrt{1 - E_{Ai}^2/\Delta^2}$. In Fig. 4, we compare the gap with the matrix elements discussed above. Here, the black solid curves are obtained by solving our effective Hamiltonian with parameters $T_{1,2} = 0.99,\ T_c = 0.3$ and $\phi_c = 0.5\,\pi$. These solutions exhibit clearly the asymmetry between δE_L and δE_R. The dip structure shown in δE_L vs ϕ_2 around $\phi_2 = 0.8\,\pi$ is due to the fact that the two gaps are merged as $\phi_2 \to \pi$. In our analysis in the ballistic limit, illustrated by blue dotted lines in Fig. 4, the mixing of the gaps is not taken into account and there is no dip structure.

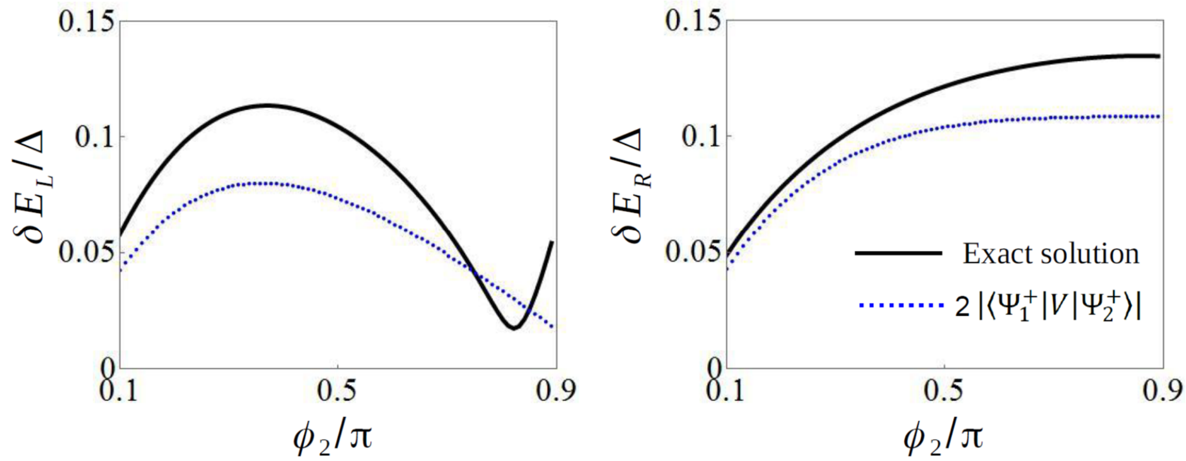

Fig. 4. *Asymmetry between left and right anti-crossing gaps as a function of ϕ_2. The solutions obtained by solving the effective Hamiltonian are drawn by black solid lines and the approximate solutions from the matrix element analyzed in the text are illustrated by blue dotted lines. Here, $\delta E_L(\phi_2 = 0.7\pi)$ and $\delta E_R(\phi_2 = 0.7\pi)$, respectively, correspond to the left and right gaps shown in Fig. 3d.*

5. Conclusions

In this deliverable, we explored theoretically a novel scheme for two Andreev qubits made by three-coupled Josephson weak links in nanowire-superconductor hybrid devices as shown in Fig. 1b and c. We studied the devices with three models – a minimal model, a microscopic tight-binding model and an effective low-energy model based on scattering theory - with the focus on the tunable coupling between the qubits. Using the minimal model, we found a simple expression of the coupling in terms of the elastic cotunneling and the crossed Andreev amplitudes, thereby showing the possibility of performing two-qubit operations. In the tight-binding model with realistic parameters, we calculated the spatial probability densities of the Andreev qubits around the level crossing point, and observed the switching of their localization from one to the other qubit as we cross the energy level crossing point. With the low-energy model, we further analyzed the dependence of the coupling on the fluxes and provided analytic expressions to explain the asymmetric coupling strength at the crossing points. In future works we shall explore this type of tunable coupling in the presence of spin-orbit coupling that could be useful for manipulating spin degree of freedom of the Andreev levels.

6. References

[Bertet2006] P. Bertet, C.J.P.M. Harmans and J.E. Mooij, "Parametric coupling for superconducting qubits", Phys. Rev. B **73,** 064512 (2006)

[Chen2014] Yu Chen, C. Neill, P. Roushan, N. Leung, M. Fang, R. Barends, J. Kelly, B. Campbell, Z. Chen, B. Chiaro, A. Dunsworth, E. Jeffrey, A. Megrant, J. Y. Mutus, P. J. J. O'Malley, C. M. Quintana, D. Sank, A. Vainsencher, J. Wenner, T. C. White, Michael R. Geller, A. N. Cleland, and John M. Martinis, "Qubit Architecture with High Coherence and Fast Tunable Coupling", Phys. Rev. Lett. **113**, 220502 (2014).

[Rigetti2005] Chad Rigetti, Alexandre Blais, and Michel Devoret, "Protocol for Universal Gates in Optimally Biased Superconducting Qubits", Phys. Rev. Lett. **94**, 240502 (2005).